Electronic Supplementary Material (ESI) for Inorganic Chemistry Frontiers.
This journal is © the Partner Organisations 2020

Supporting Information for:

Observing the Three-Dimensional Dynamics of Supported Metal Complexes

Alexander L. Paterson,[1] Da-Jiang Liu,[1] Uddhav Kanbur,[1,2] Aaron D. Sadow,[1,2] Frédéric A. Perras[1]*

[1]US DOE, Ames Laboratory, Ames, IA 50011 USA
[2]Department of Chemistry, Iowa State University, Ames, IA 50011 USA

*Author to whom correspondence should be addressed
fperras@ameslab.gov

Additional Details on the GIPAW DFT Calculations

Density functional theory (DFT) calculations using the exchange-correlation functional of Perdew, Burke, and Ernzerhof (PBE)[1] are well-known to overestimate the hybridization of 2p orbitals of atoms neighboring those with empty d or f orbitals. This was first and perhaps best shown by Profeta *et al*. for the pairing of Ca^{2+} and O^{2-} in calcium oxides,[2] but this effect can be demonstrated in many of the rare earths (Sc, Y, La),[3] and is not limited to cases where O^{2-} is the neighboring atom.[4] This spurious hybridization affects the calculated isotropic shielding of both species. Per Profeta *et al*., the spurious hybridization can be mitigated by shifting the empty d or f orbital to a higher energy.[2] DFT+*U* can be used to similar effect.[3]

Regardless of which method is used, the choice of how much energy shift to apply is important. There is no inherent *a priori* choice for the energy level correction. In order to constrain our shift of the Sc 3d energy level, we follow the method used by Jaworski *et al*.[3] To summarize, we first construct a calibration curve relating ^{17}O shieldings (σ_{iso}) and chemical shifts (δ_{iso}) for compounds which should be unaffected by the spurious hybridization (Figure S1). We then shift the Sc 3d orbital energy until the Sc_2O_3 ^{17}O data point lies on the calibration curve (Figure S2). To cross-check the validity of the correction, we then compare the shielding-shift relationship for the two crystallographically-inequivalent Sc sites in Sc_2O_3; if the Sc 3d energy level shift is correct, the two Sc sites should be fit by a line with the slope of -1 (Figure S3).

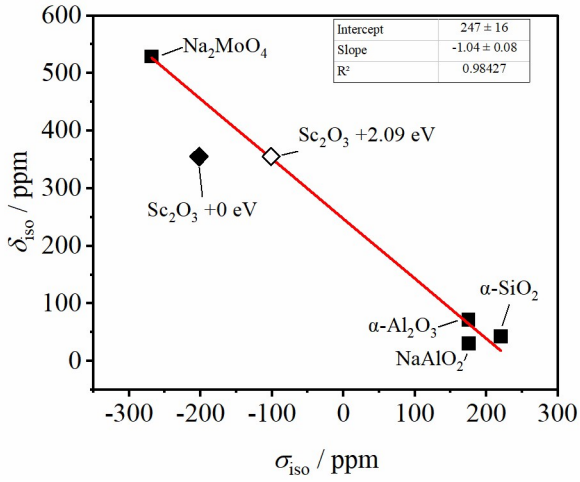

Figure S1. Experimental ^{17}O isotropic chemical shifts (δ_{iso}) and their corresponding calculated isotropic shieldings (σ_{iso}). The reference structures are presented as squares. The Sc_2O_3 value from the uncorrected calculation is a black diamond, while that from the corrected (+2.09 eV) calculation is a white diamond. The reference compounds used for the calibration correspond to α-Al_2O_3,[5,6] α-SiO_2,[7,8] Na_2MoO_4,[9,10] $NaAlO_2$,[11,12] and Sc_2O_3[13,14].

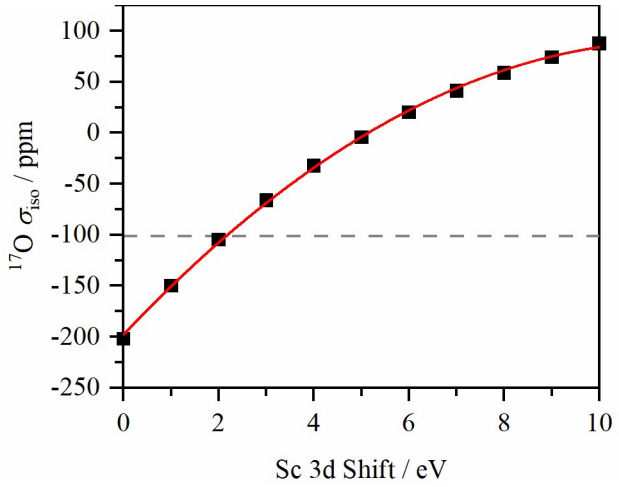

Figure S2. The change in the calculated ^{17}O σ_{iso} of Sc_2O_3 in response to changes in the shift of the Sc 3d energy level. The dashed grey line corresponds to the expected ^{17}O σ_{iso} value (Figure S1). The red line is a parabolic fit to the data.

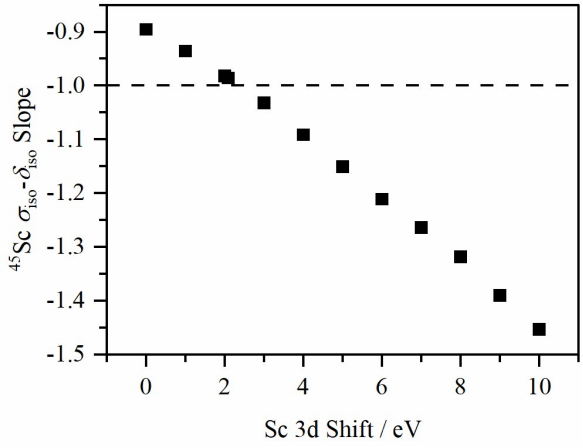

Figure S3. The slope of the line connecting the experimental ^{45}Sc δ_{iso} and calculated ^{45}Sc σ_{iso} values for the two crystallographically-inequivalent Sc sites in Sc_2O_3 as a function of the Sc 3d USPP energy shift. A dashed line is drawn at -1.0 for visual reference.

Following the above approach, we find that a shift of +2.09 eV to the Sc 3d orbital in the Sc ultrasoft pseudopotential (USPP) both moves the Sc_2O_3 ^{17}O σ_{iso} to the appropriate value in the calibration curve, and yields a Sc_2O_3 ^{45}Sc δ_{iso} vs. σ_{iso} relationship with a slope of -0.99. We thus use this shift for all GIPAW calculations on our Sc-containing compounds.

Note that we have only discussed the effect of the Sc 3d energy shift on the shielding tensor, and not the electric field gradient tensor. We find that while increasing the energy shift leads to *more negative* quadrupolar coupling constants (C_Q), the overall effect is small, changing the C_Q by less than 2% at the +2.09 eV level we used.

The string used for generation of the USPP within CASTEP is as follows:

Sc 3|1.8|11|13.5|15.1|30U:40UU:31UU:32U@0.0768U@0.0768(qc=6.5)[]

The Drawing of Thermal Ellipsoids

To map the dynamics of the *i*Pr groups using thermal ellipsoids, we first found the narrowest range of dihedral angles encompassing 50% of the values from the histogram in Figure 10d. The atoms are then repositioned to the center on this range and the C-X (X being either C or H) bond length (b) is reduced by a factor of (1-cosϕ)/2, where ϕ is the amplitude of the libration range, see Figure 11. The width of the ellipsoid in the direction of the bond is of b(1-cosϕ) and that in the direction of libration is 2$b$sinϕ. To visualize the ellipsoids using crystallographic software, these numbers must be squared to comply with the Å^2 convention and it is necessary to rotate them in the proper direction. The eigenvector for the first component is the C-X bond vector and the eigenvector for the second component can be calculated by performing the cross-product between the first eigenvector and N-C bond vector. The third eigenvector is obtained by performing the cross-product between the other two eigenvectors. These three eigenvectors can be organized into the columns of a matrix **P**, with which it is possible to calculate the components of the displacement tensor **U** in the crystal frame.

$$U = P\begin{bmatrix} b^2(1-cos\phi)^2 + U_{iso} & 0 & 0 \\ 0 & 4b^2sin^2\phi + U_{iso} & 0 \\ 0 & 0 & U_{iso} \end{bmatrix}P^T$$

The isotropic displacement U_{iso} was set to 0.04 Å^2. See Figure S4 for further clarification.

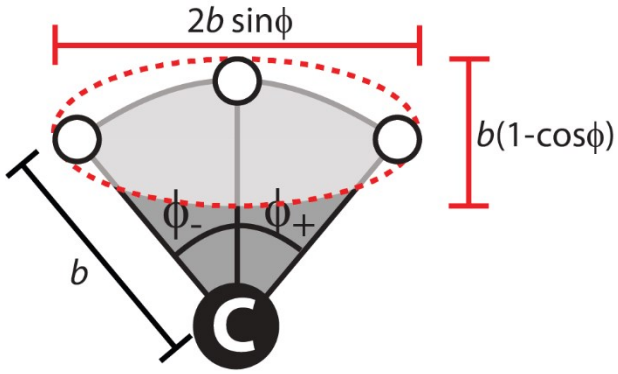

Figure S4. Depiction of the eigenvectors of the **U** tensor and the thermal ellipsoid for a partial rotation about a particular bond.

Supplementary Tables and Figures

Table S1. GIPAW-calculated values for the DFT-optimized structures described in the main manuscript. Averages of these values are reported in Table 1.

Structure[a]	Surface location	δ_{iso} / ppm[b]	σ_{iso} / ppm	C_Q / MHz[c]	η
1	1	167.41	706.86	8.13	0.57
2	1	161.62	712.65	-26.44	0.66
2	2	174.16	700.11	-33.59	0.49
2	3	170.81	703.46	-29.54	0.69
2	4	198.60	675.67	-28.76	0.14
2	5	226.57	647.70	-49.50	0.32
3	1	239.09	635.18	38.23	0.90
3	2	235.04	639.23	41.57	0.84
3	3	249.78	624.49	49.91	0.59
4	1	136.22	738.05	-21.71	0.33
4	2	131.34	742.93	-24.73	0.30
4	3	137.80	736.47	-22.76	0.39

[a]See Figure 4 in the main text. [b]Calculated δ_{iso} values were obtained using an absolute shielding constant (σ_{ref}) of 874.26 ppm, which was calculated using Sc_2O_3. [c]Calculated C_Q values were obtained using a nuclear quadrupole moment of -220 mb.[15]

Table S2. GIPAW-calculated values for snapshots of the molecular dynamics simulation performed on **2**. Averages of these values are reported in Table 1.

Time step index	δ_{iso} / ppm[a]	σ_{iso} / ppm	C_Q / MHz[b]	η
5019	191.64	681.63	15.89	0.87
5209	199.32	674.95	-18.43	0.74
5283	186.29	687.98	21.61	0.64
6868	203.26	671.01	-35.92	0.60
7606	212.75	661.52	-15.43	0.87
7990	231.37	642.90	-20.16	0.74
8175	187.99	686.28	17.21	0.96
8234	205.39	668.88	18.36	0.96
8979	205.98	668.29	-17.83	0.44
9504	188.78	685.49	-28.57	0.56
5166			-18.30	0.71
5188			28.88	0.91
5239			26.53	0.46
5280			-16.02	0.54
5289			-14.92	0.69
5329			-28.96	0.98
5352			-21.00	0.56
5458			12.17	0.69
5862			-21.17	0.55
5893			-19.20	0.18
5902			-13.44	0.83

5945	-20.13	0.36
5958	-22.89	0.50
6142	-15.39	0.36
6150	-24.79	0.84
6520	-25.55	0.18
6583	25.52	0.31
6692	-22.71	0.42
6765	-14.44	0.26
6792	-30.69	0.77
6870	-37.60	0.78
6910	-36.23	0.48
7054	18.71	0.71
7239	-22.31	0.60
7313	-25.15	0.59
7327	-34.41	0.23
7360	-21.18	0.81
7410	-18.79	0.66
7495	23.00	0.89
7527	-35.47	0.77
7630	17.96	0.91
7692	14.11	0.94
7848	-17.89	0.56
8049	-18.45	0.72
8062	-32.72	0.90
8280	-26.63	0.35
8294	19.91	0.51
8658	-25.37	0.63
8856	-25.62	0.34
8982	-20.09	0.19
9030	-16.36	0.65
9042	-25.25	0.52
9132	26.02	0.98
9208	30.54	0.73
9372	-25.12	0.44
9656	16.27	0.24
9670	28.52	0.24
9774	-26.36	0.53
9871	-24.63	0.46
9954	32.43	0.47

[a] Calculated δ_{iso} values were obtained using an absolute shielding constant (σ_{ref}) of 874.26 ppm, which was calculated using Sc_2O_3. [b]Calculated C_Q values were obtained using a nuclear quadrupole moment of -220 mb.[15]

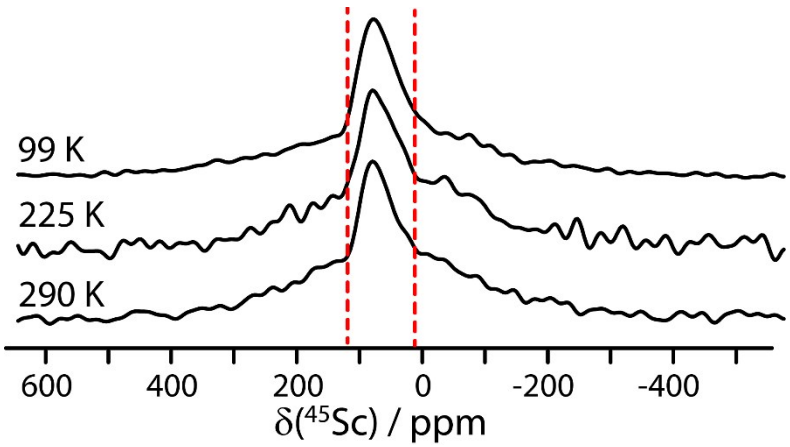

Figure S5. Variable temperature ^{45}Sc MAS NMR spectra of the grafted complex **2** acquired with an MAS frequency of 12.5 kHz at the temperature indicated on the Figure. The lineshape is not significantly affected by temperature, in agreement with our observation, from ^{1}H-^{13}C dipolar coupling measurements, that there are no large amplitude motions about the O-Sc bond.

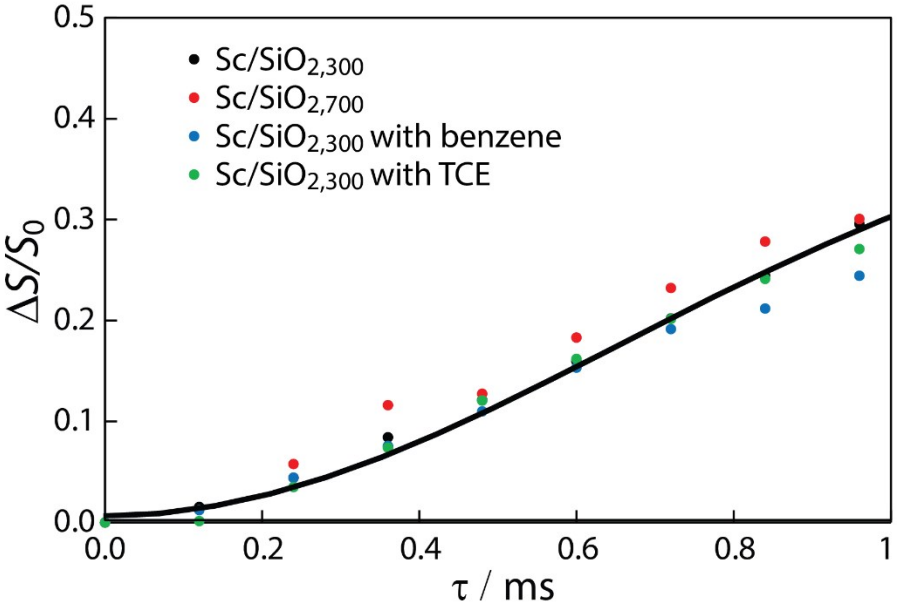

Figure S6. ^{1}H{^{45}Sc} RESPDOR dephasing curves measured for the amidinate ^{1}H site of complex **1** grafted on silica pre-treated at 300 °C ($Sc/SiO_{2,300}$) and 700 °C ($Sc/SiO_{2,700}$) as well as the former wetted with benzene and TCE, as indicated on the Figure. A simulated curve is shown corresponding to an H-Sc order parameter of 1. Only the first millisecond is shown as the later time points are affected by spinning instabilities for some samples.

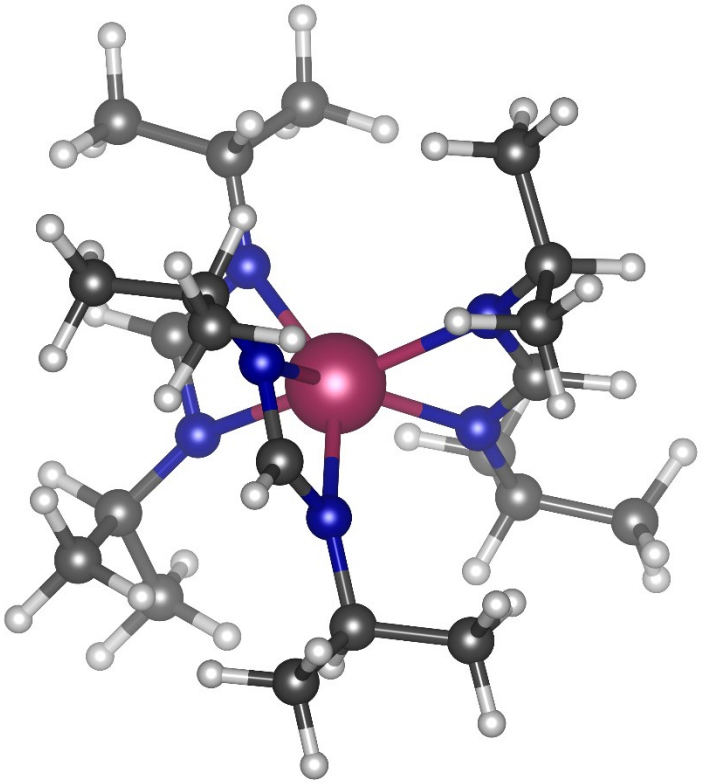

Figure S7. DFT-optimized structure of the scandium amidinate complex.

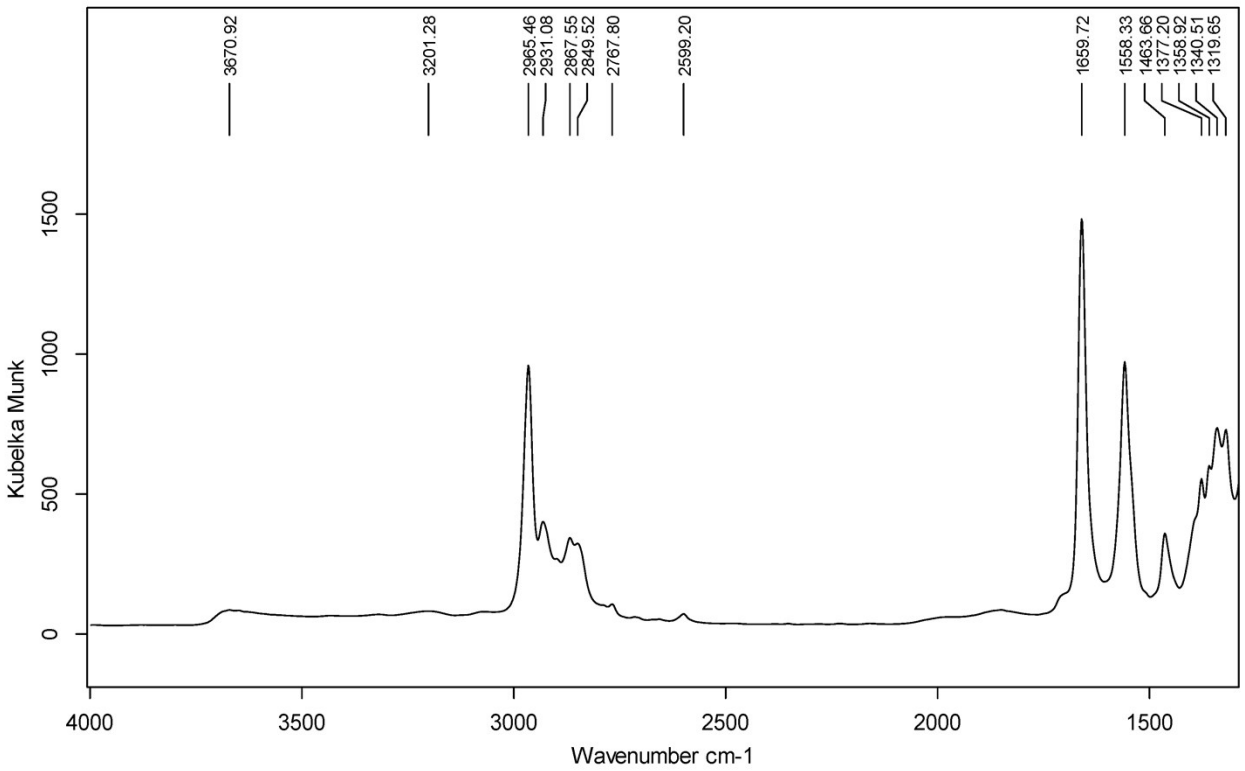

Figure S8. DRIFTS spectrum of the SiO_2-supported complex Sc amidinate complex.

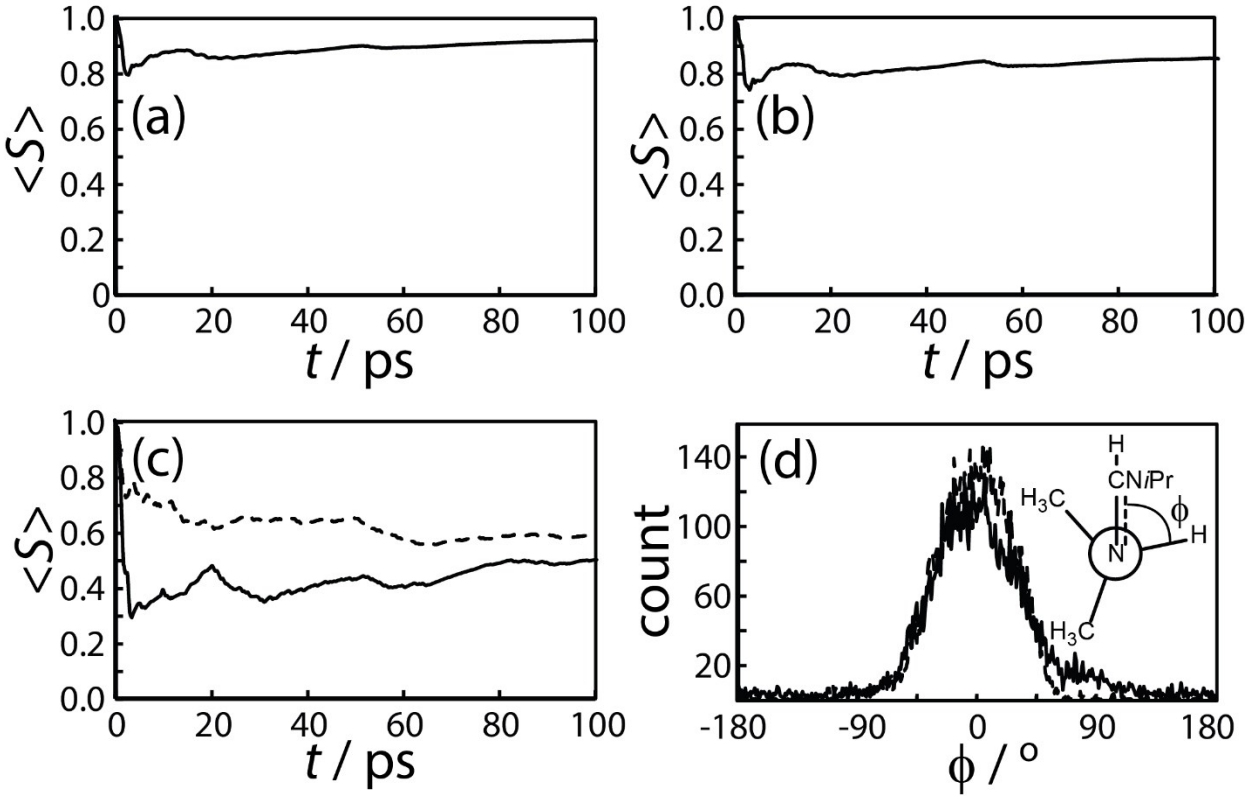

Figure S9. Results from the DFT-MD simulation of complex **3**. The order parameters for the ^{45}Sc-amidinate ^{1}H dipolar coupling (a), the amidinate ^{13}C{^{1}H} dipolar coupling (b), and *i*Pr ^{13}C{^{1}H} dipolar coupling (c) are shown as a function of the simulation time. The methyl ^{13}C{^{1}H} order parameters are not shown given that a longer simulation time is needed to perform full methyl rotations, instead it can be assumed to be 1/3 of the value in (c). Dashed and solid lines in (c) and (d) correspond to opposing *i*Pr moieties from the same ligand. In (d) the histograms of the *i*Pr-CH and amidinate N-C dihedral angle (ϕ) are shown.

---

[1] J. P. Perdew, K. Burke, M. Ernzerhof, Generalized gradient approximation made simple. *Phys. Rev. Lett.* 1996, **77**, 3865-3868.

[2] M. Profeta, M. Benoit, F. Mauri, C. J. Pickard, First-principles calculation of the ^{17}O NMR parameters in Ca oxide and Ca aluminosilicates: The partially covalent nature of the Ca−O bond, a challenge for density functional theory. *J. Am. Chem. Soc.* 2004, **126**, 12628-12635.

[3] A. Jaworski, T. Charpentier, B. Stevensson, M. Edén, Scandium and yttrium environments in aluminosilicate glasses unveiled by ^{45}Sc/^{89}Y NMR spectroscopy and DFT calculations: what structural factors dictate the chemical shifts? *J. Phys. Chem. C*, 2017, **121**, 18815-18829.

[4] A. Sadoc, M. Body, C. Legein, M. Biswal, F. Fayon, X. Rocquefelte, F. Boucher, NMR parameters in alkali, alkaline earth and rare earth fluorides from first principle calculations. *Phys. Chem. Chem. Phys.* 2011, **13**, 18539-18550.

[5] S. Kondo, K. Tateishi, N. Ishizawa, structural evolution of corundum at high temperatures. *Jpn. J. Appl. Phys.* 2008, **47**, 616-619.

[6] P. Florian, M. Gervais, A. Douy, D. Massiot, J.-P. Coutures, A multi-nuclear multiple-field nuclear magnetic resonance study of the Y_2O_3-Al_2O_3 phase diagram. *J. Phys. Chem. B* 2001,

105, 379-391.
[7] H. D'Amour, W. Denner, H. Schulz, Structure determination of α-quartz up to 68 × 10^8 Pa. *Acta Cryst* 1979, **B35**, 550-555.
[8] F. H. Larsen, I. Farnan, ^{29}Si and ^{17}O (Q)CPMG-MAS solid-State NMR experiments as an optimum approach for half-integer nuclei having long T_1 relaxation times. *Chem. Phys. Lett.* 2002, **357**, 403-408.
[9] K. G. Bramnik, H. Ehrenberg, Study of the Na_2O—MoO_3 system. $Na_6Mo_{11}O_{36}$ — a new oxide with anatase-related structure, and the crystal structures of Na_2MoO_4. *Z. Anorg. Allg. Chem.* 2004, **630**, 1336-1341.
[10] E. Farkas, H. Csóka, I. Tóth, new insights into the solution equilibrium of molybdenum(VI)-hydroxamate systems: ^{1}H and ^{17}O NMR spectroscopic study of Mo(VI)-desferrioxamine B and Mo(VI)-monohydroxamic acid systems. *Dalton Trans.*, 2003, 1645-1652.
[11] A. F. Reid and A. E. Ringwood, High-pressure $NaAlO_2$, an α-$NaFeO_2$ isotype. *Inorg. Chem.* 1968, **7**, 443-445.
[12] R. M. Hazen, H. Yang, L. W. Finger, B. A. Fursenko, Crystal chemistry of high-pressure $BaSi_4O_9$ in the trigonal (*P*3) barium tetragermanate structure. *Am. Mineral.* 1999, **84**, 987-989.
[13] O. Knop, J. M. Hartley, Refinement of the crystal structure of scandium oxide. *Can. J. Chem.* 1968, **46**, 1446-1450.
[14] E. Oldfield, C. Coretsopoulos, S. Yang, L. Reven, H. C. Lee, J. Shore, O. H. Han, E. Ramli, D. Hinks, ^{17}O nuclear-magnetic-resonance spectroscopic study of high-T_c superconductors. *Phys. Rev. B* 1989, **40**, 6832.
[15] P. Pyykkö, P. Year-2017 Nuclear Quadrupole Moments. *Mol. Phys.* 2018, **116**, 1328-1338.